USGS
science for a changing world

Hydrothermal Alteration Maps of the Central and Southern Basin and Range Province of the United States Compiled From Advanced Spaceborne Thermal Emission and Reflection Radiometer (ASTER) Data

By John C. Mars

Open-File Report 2013–1139
Version 1.1, April 8, 2014

U.S. Department of the Interior
U.S. Geological Survey

U.S. Department of the Interior
SALLY JEWELL, Secretary

U.S. Geological Survey
Suzette M. Kimball, Acting Director

U.S. Geological Survey, Reston, Virginia: 2013
Revised: April 8, 2014

Suggested citation:
Mars, J.C., 2013, Hydrothermal alteration maps of the central and southern Basin and Range province of the United States compiled from Advanced Spaceborne Thermal Emission and Reflection Radiometer (ASTER) data (ver 1.1, April 8, 2014: U.S. Geological Survey Open-File Report 2013–1139, 6 p., 13 plates, scale 1:1,300,000, *http://dx.doi.org/10.3133/ofr20131139*.

ISSN 2331-1258 (online)

Contents

Figures

Plates

[Available separately at *http://pubs.usgs.gov/of/2013/1139/plates*.]

Table

Conversion Chart

Multiply	By	To obtain
	Length	
micrometer (μm)	0.00003937	inch (in.)
meter (m)	3.281	foot (ft)
kilometer (km)	0.6214	mile (mi)

Vertical coordinate information is referenced to the National Geodetic Vertical Datum of 1984.

Horizontal coordinate information is referenced to the 1927 North American Datum.

The resolution of pixels in spatial datasets follows the conventions used in the spatial data and modeling communities. The format is "n-meter resolution," where n is a numerical value for the length. The usage translates into a pixel with a length of n on all sides that covers an area of n meters × n meters.

Hydrothermal Alteration Maps of the Central and Southern Basin and Range Province of the United States Compiled From Advanced Spaceborne Thermal Emission and Reflection Radiometer (ASTER) Data

By John C. Mars

Abstract

Advanced Spaceborne Thermal Emission and Reflection Radiometer (ASTER) data and Interactive Data Language (IDL) logical operator algorithms were used to map hydrothermally altered rocks in the central and southern parts of the Basin and Range province of the United States. The hydrothermally altered rocks mapped in this study include (1) hydrothermal silica-rich rocks (hydrous quartz, chalcedony, opal, and amorphous silica), (2) propylitic rocks (calcite-dolomite and epidote-chlorite mapped as separate mineral groups), (3) argillic rocks (alunite-pyrophyllite-kaolinite), and (4) phyllic rocks (sericite-muscovite). A series of hydrothermal alteration maps, which identify the potential locations of hydrothermal silica-rich, propylitic, argillic, and phyllic rocks on Landsat Thematic Mapper (TM) band 7 orthorectified images, and ArcGIS[1] shape files of hydrothermal alteration units are provided in this study.

Introduction

Advanced Spaceborne Thermal Emission and Reflection Radiometer (ASTER) data were used to compile 12 maps (plates 1, 2*A–F*, 3*A–F*; fig.1) that illustrate minerals associated with hydrothermal alteration in the central and southern parts of the Basin and Range province of the United States. ASTER data consist of reflected radiation measurements in three bands in the visible and near-infrared-wavelength (VNIR) region from 0.52 to 0.86 micrometers (μm); six bands in the 1.6- to 2.43-μm short-wave-infrared-wavelength (SWIR) region; and five bands of emitted radiation in the 8.125- to 11.65-μm thermal-infrared-wavelength (TIR) region with 15-meter (m), 30-m, and 90-m resolution, respectively (Fujisada, 1995). The ASTER instrument also has a backward-looking VNIR telescope with 15-m resolution and a swath width of 60 kilometers (km) (Fujisada, 1995).

Economic deposits such as gold and copper are typically associated with hydrothermally altered rocks (John and others, 2010), which typically consist of one or more hydrous zones of alteration minerals containing at least one mineral that exhibits diagnostic spectral absorption features in the VNIR through the SWIR and (or) the thermal-infrared TIR regions (Ashley, 1979; Abrams and others, 1983; Hunt and Spatz and Wilson, 1995). ASTER bands are positioned to define and map the diagnostic VNIR, SWIR, and TIR spectral absorption features of hydrothermal alteration minerals (Rowan and Mars, 2003; Rowan and others, 2003; Mars and Rowan, 2006).

[1]ESRI, Redlands, Calif.

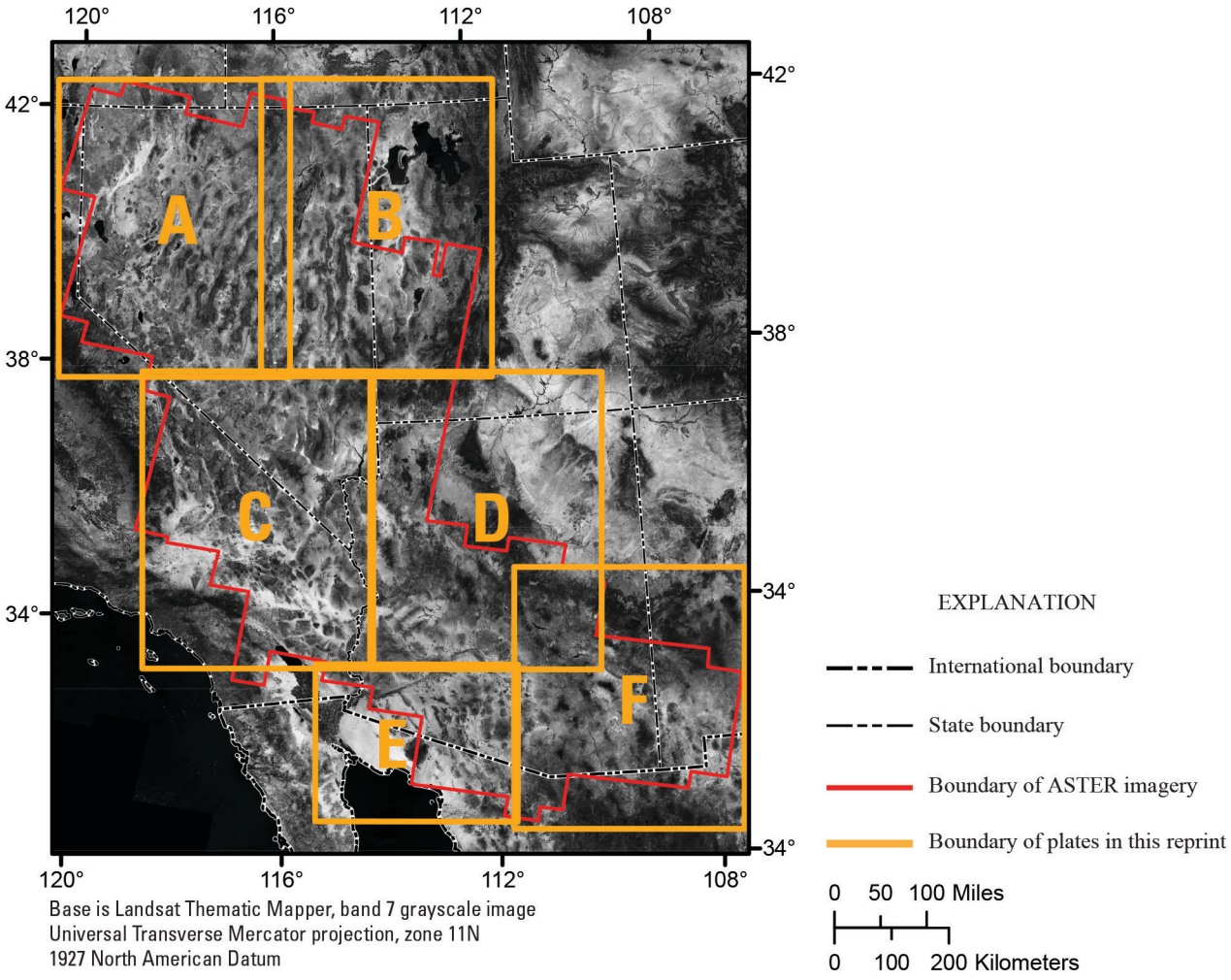

Figure 1. Index map showing coverage for the hydrothermal alteration maps of the central and southern Basin and Range province of the United States compiled from Advanced Spaceborne Thermal Emission and Reflection Radiometer (ASTER) data and the locations of plates 2*A–F* and 3*A–F*.

Data and Processing Methods

The ASTER dataset used to cover the central and southern parts of the Basin and Range province in the United States consists of 247 ASTER_Level 1B scenes (plate 1). The ASTER_Level 1B radiance data consist of all VNIR, SWIR and TIR bands, including the backward-looking VNIR band. The VNIR and SWIR radiance data were calibrated to the reflectance data using Moderate Resolution Imaging Spectrometer (MODIS) water-vapor data, radiometric "crosstalk" correction software, radiance "gain" correction coefficients, and Atmospheric Correction Now (ACORN)[2] software (ImSpec LLC, 2004; Biggar and others, 2005; Iwasaki and Tonooka, 2005; ITT, 2008; Mars and Rowan, 2010). The TIR radiance data were calibrated to emissivity using atmospheric removal and emissivity normalization algorithms in Environment for Visualizing Images (ENVI)[3], an image calibration and processing

[2]ImSpec, LLC, Palmdale, Calif.
[3]Exelis Visual Information Services (formerly ITT), Boulder, Colo.

software package (ITT, 2008). Each ASTER scene was georectified to a Landsat TM 30-m orthorectified image with a root mean square error of less than 60 m (Tucker and others, 2005).

Rocks containing hydrous quartz, chalcedony, opal, and amorphous silica (hydrothermal silica-rich rocks), calcite-dolomite and epidote-chlorite (propylitic), alunite-pyrophyllite-kaolinite (argillic), and sericite-muscovite (phyllic) were mapped using Interactive Data Language (IDL) logical operators (table 1). The IDL logical operators consist of band thresholds and band ratios strung together to map spectral absorption features of minerals (table 1; Mars and Rowan 2006; John and others, 2010). All of the logical operator algorithms mask green vegetation using a ratio of VNIR band 3/band 2, which detects the chlorophyll absorption feature at 0.67 μm (table 1). In addition, a band 4 threshold is used to mask low signals, and thus noisy spectra (table 1).

Table 1. Interactive Data Language (IDL) logical operator algorithms used with Advanced Spaceborne Thermal Emission and Reflection (ASTER) Radiometer data to map hydrothermally altered rocks in the central and southern parts of the Basin and Range province of the United States.

[Algorithm notations follow usage of Mars and Rowan (2006). b, band; float, floating point; le, less than or equal to; lt, less than; ge, greater than or equal to; gt, greater than]

Hydrothermally altered rock	Algorithm
Hydrothermal silica-rich (hydrous silica, chalcedony, opal)	((float(b3)/b2) le 1.55) and (b4 gt 2400) and ((float(b4)/b7)ge 1.413) and ((float(b13)/b12) ge 1.025) and ((float(b12)/b11) lt 1.02)
Propylitic (carbonate)	((float(b3)/b2) le 1.55) and b4 gt 2600 and (float(b6) / b8 gt 1.162) and (b5 gt b6) and (b7 gt b8) and (b9 gt b8) and ((float(b13) / b14) gt 1.005)
Propylitic (epidote-chlorite)	((float(b3)/b2) le 1.55) and b4 gt 2600 and (float(b6) / b8 gt 1.162) and (float(b5) / (float(b4)+b6) gt 0.456) and (b5 gt b6) and (b6 gt b7) and (b7 gt b8) and (b9 gt b8) and ((float(b13) / b14) le 0.999)
Argillic (alunite, kaolinite)	((float(b3)/b2) le 1.55) and (b4 gt 2600) and ((float(b4)/b6) gt 1.492) and ((float(b5)/b6) le 1.105) and ((float(b7)/b6) ge 1.03)
Phyllic (sericite-muscovite)	((float(b3)/b2) le 1.55) and (b4 gt 2600)and ((float(b4)/b6) gt 1.492) and ((float(b5)/b6) gt 1.105) and ((float(b7)/b6) ge 1.03)

Hydrothermally altered phyllic and argillic rocks were mapped using ASTER VNIR and SWIR data at 30-m spatial resolution. SWIR band ratios were used in IDL logical operators to map Al-O-H spectral absorption features associated with alunite, kaolinite, and sericite-muscovite. The ratio of SWIR band 4/band 5 maps the 2.165-μm spectral absorption feature associated with alunite, pyrophyllite, and kaolinite, and the ratios of SWIR band 4/band 6 and band 7/band 6 map the 2.2-μm spectral absorption feature exhibited by alunite, kaolinite, and sericite (table 1).

Hydrothermal silica-rich rocks were mapped using ASTER SWIR and TIR band ratios at 90-m resolution (table 1). The ratio of SWIR band 4/band 7 is typically higher for hydrothermal silica-rich rocks, which have lower overall SWIR reflectance in the 2.0- to 2.4-μm region than nonhydrothermal silica-rich rocks because of residual molecular water or an O-H absorption feature spanning 2.26 to 2.4 μm. The ratio of TIR band 13/band 12 maps the 9.09-μm quartz reststrahlen absorption feature. Thus, silica-rich rocks were mapped using the TIR emissivity data and hydrothermal silica-rich rocks were discriminated from the non-hydrothermal silica-rich rocks using the corresponding SWIR reflectance data for each pixel.

Hydrothermally altered propylitic rocks were mapped using ASTER SWIR and TIR band ratios at 90-m spatial resolution (table 1). Calcite, dolomite, epidote, and chlorite typically exhibit overlapping CO_3 and Fe,Mg-O-H spectral absorption features at 2.31 to 2.33 μm and have been difficult to map separately using SWIR data in previous studies (Dalton and others, 2004). In the TIR region, however,

rocks containing calcite and dolomite exhibit an 11.2-μm spectral absorption feature, whereas epidote- and chlorite-rich rocks have TIR spectral absorption features centered at approximately 10.2 μm. Thus, TIR calcite-dolomite spectra exhibit higher band-13 emissivity and lower band-14 emissivity, whereas epidote-chlorite TIR spectra exhibit lower band-13 emissivity and higher band-14 emissivity. The calcite-dolomite and epidote-chlorite logical operators use the ratio of SWIR band 6/band 8 to map the 2.31- to 2.33-μm absorption feature of both groups of minerals and the ratio of TIR band 13/band 14 set to greater than 1.005 to separate and map calcite-dolomite-rich rocks and less than 0.999 to separate and map epidote-chlorite-rich rocks (table 1).

The argillic and phyllic units are mapped at 30-m spatial resolution and the hydrothermal silica-rich rocks and propylitic units are mapped at 90-m spatial resolution. Each logical operator algorithm produces an image with pixel values of one or zero which is converted to a polygon-based shape file for import into ArcGIS. The logical operators correctly mapped (with ±20 percent error) hydrothermal alteration at three calibration-validation test sites on the basis of field data and mineral maps compiled from previous studies (the Cuprite area of Nevada; Mountain Pass, California; and Yerington, Nevada; Mars and Rowan, 2010).

Map Description

Mineral-group units illustrated on the maps include phyllic (muscovite, sericite), argillic (alunite, kaolinite, pyrophyllite), propylitic (epidote, chlorite), a second propylitic unit (calcite, dolomite), and hydrothermal silica-rich rocks (hydrous quartz, chalcedony, opal, amorphous silica; plates 2*A–F,* 3*A–F*). Rocks or sediment that contain significant amounts of any of these minerals are mapped as one of the mineral-group units, including rocks and sediment not associated with hydrothermal alteration such as playa-lake sediments and sedimentary rocks rich in detrital clays and muscovite, sedimentary limestone and dolomite, and muscovite-clay-rich sandstone and conglomerates (which may also be classified on the map as hydrothermal silica-rich rocks). Mineral-group units are illustrated on a Landsat TM band 7 mosaic at 30-m spatial resolution (plates *2A–F, 3A–F;* Tucker and others, 2005).

As shown in previous studies, hydrothermally altered rocks must be identified on the basis of (1) the types and patterns of minerals associated with hydrothermal alteration and (2) rocks associated with the mapped mineral groups (Mars and Rowan, 2006; John and others, 2010). Previous studies have shown that hydrothermal alteration is typically associated with igneous rocks, and patterns of hydrothermal alteration are typically circular to elliptical for porphyry systems and linear for epithermal-vein hydrothermal systems (Mars and Rowan, 2006; John and others, 2010). Thus, rock types and spatial patterns of the map units must also be considered in identifying hydrothermally altered rocks. ArcGIS shape files of each hydrothermally altered unit are provided with this study[4] and may be used in conjunction with geographic information system (GIS)-based lithologic databases, which contain maps of igneous rocks for Arizona, California, Nevada, and New Mexico and are available over the Internet (Ludington and others, 2007; Stoeser and others, 2007).

Field investigations and geologic and mineral maps of the Cuprite area and Mountain Pass from previous studies showed that hydrothermal silica-rich rocks are typically mixed with phyllic- and argillic-rich rocks, with some minor mixing of hydrothermal silica-rich rocks with epidote-chlorite- and carbonate-rich rocks (Ashley and Abrams, 1980; Rowan and Mars, 2003; Rowan and others, 2003; Mars and Rowan, 2010). Thus, in order to show all mineral units mapped in an area, hydrothermal silica-rich, argillic, phyllic, and propylitic rocks are displayed on one set of maps (plates 2*A–F*) and all

[4] Data may be accessed at http://mrdata.usgs.gov/surficial-mineralogy/ofr-2013-1139/.

hydrothermally altered units except for hydrothermal silica-rich rocks are displayed for the same area on a second set of maps (plates 3*A–F*).

References Cited

Abrams, M.J., Brown, L., Lepley, R., and Sadowski, P., 1983, Remote sensing for porphyry copper deposits in Southern Arizona: Economic Geology, v. 78, p. 591–604.

Biggar, S.F., Thome, K.J., McCorkel, J.T., and D'Amico, J.M., 2005, Vicarious calibration of the ASTER SWIR sensor including crosstalk correction: Proceedings, International Society of Optical Engineering, v. 5882, p. 17.

Dalton, J.B., Bove, D.J., Mladinich, C.S., and Rockwell, B.W., 2004, Identification of spectrally similar materials using the USGS tetracorder algorithm; the calcite-epidote-chlorite problem: Remote Sensing of Environment, v. 89, p. 455–466.

Fujisada, H., 1995, Design and performance of ASTER instrument: Proceedings of the International Society for Optical Engineering, v. 2583, p. 16−25.

Hunt, G.R., and Ashley, R.P., 1979, Spectra of altered rocks in the visible and near infrared: Economic Geology, v. 74, no. 7, p. 1613–1629.

ImSpec, LLC, 2004, ACORN 5.0 tutorial manual: Pasadena, Calif., ImSpec, LLC, 143 p.

ITT, 2008, The Environment for Visualizing Images (ENVI) software: Boulder, Colo., ITT Visual Information Solutions, accessed August 15, 2011, at http://www.ittvis.com/ProductServices/ENVI.aspx.

Iwasaki, A., and Tonooka, H., 2005, Validation of a crosstalk correction algorithm for ASTER/SWIR: IEEE Transactions on Geoscience and Remote Sensing, v. 43, no. 12, p. 2747–2751.

John, D.A., Ayuso, R.A., Barton, M.D., Blakely, R.J., Bodnar, R.J., Dilles, J.H., Gray, Floyd, Graybeal, F.T., Mars, J.C., McPhee, D.K., Seal, R.R., Taylor, R.D., and Vikre, P.G., 2010, Porphyry copper deposit model, chap. B *of* Mineral deposit models for resource assessment: U.S. Geological Survey Scientific Investigations Report 2010–5070–B, 169 p., available only at http://pubs.usgs.gov/sir/2010/5070/b/.

Ludington, Steve, Moring, B.C., Miller, R.J., Stone, P.A., Bookstrom, A.A., Bedford, D.R., Evans, J.G., Haxel, G.A., Nutt, C.J., Flyn, K.S., and Hopkins, M.J., 2007, Preliminary integrated geologic map databases for the United States; Western States; California, Nevada, Arizona, Washington, Oregon, Idaho, and Utah, version 1.2: U.S. Geological Survey Open-File Report 2005–1305, available only at http://pubs.usgs.gov/of/2005/1305/.

Mars, J.C., and Rowan, L.C., 2006, Regional mapping of phyllic- and argillic-altered rocks in the Zagros magmatic arc, Iran, using Advanced Spaceborne Thermal Emission and Reflection Radiometer (ASTER) data and logical operator algorithms: Geosphere, v. 2, p. 161–186, 2 plates, doi:10.1130/GES00044.1.

Mars, J.C., and Rowan, L.C., 2010, Spectral assessment of new ASTER SWIR surface reflectance data products for spectroscopic mapping of rocks and minerals: Remote Sensing of Environment, v. 114, p. 2011–2025.

Rowan, L.C., Hook, S.J., Abrams, M.J., and Mars, J.C., 2003, Mapping hydrothermally altered rocks at Cuprite, Nevada, using the Advanced Spaceborne Thermal Emission and Reflection Radiometer (ASTER), a new satellite-imaging system: Economic Geology, v. 98, no. 5, p. 1019–1027.

Rowan, L.C., and Mars, J.C., 2003, Lithologic mapping in the Mountain Pass, California area using Advanced Spaceborne Thermal Emission and Reflection Radiometer (ASTER) data: Remote Sensing of Environment, v. 84, no. 3, p. 350–366.

Spatz, D.M., and Wilson, R.T., 1995, Remote sensing characteristics of porphyry copper systems, western American Cordillera, *in* Pierce, F.W., and Bolm, J.G., eds., Porphyry copper deposits of the American Cordillera: Arizona Geological Society Digest, v. 20, p. 94–108.

Stoeser, D.B., Green, G.N., Morath, L.C., Heran, W.D., Wilson, A.B., Moore, D.W., and Van Gosen, B.S., 2007, Preliminary integrated geologic map databases for the United States; Central States; Montana, Wyoming, Colorado, New Mexico, North Dakota, South Dakota, Nebraska, Kansas, Oklahoma, Texas, Iowa, Missouri, Arkansas, and Louisiana, U.S. Geological Survey Open-File Report 2005–1351, available only at http://pubs.usgs.gov/of/2005/1351/.

Tucker, C.J., Grant, D.M., and Dykstra, J.D., 2005, NASA's global orthorectified Landsat dataset: Photogrammetric Engineering and Remote Sensing, v. 70, p. 313–322.

ISSN 2331-1258
DOI URL http://dx.doi.org/10.3133/139